Modeling of natural fracture initiation and propagation in basin sedimentation context

Zady Ouraga, Nicolas Guy, Amade Pouya

Modeling of natural fracture initiation and propagation in basin sedimentation context

Z. Ouraga[1,2]*, **N. Guy**[1], **A. Pouya**[2]

[1]IFP Energies Nouvelles, 1 et 4 avenue du Bois-Préau, 92852, Rueil-Malmaison, France.
[2]Université Paris-Est, Laboratoire Navier (UMR 8205), CNRS, Ecole des Ponts ParisTech, IFSTTAR 77455 Marne la vallée, France.

Key Points:

- Basin modeling
- Overpressures
- Geomechanics
- Natural fracture
- Cohesive joint
- Damage

*Current address, 1 et 4 avenue du Bois-Préau, 92852, Rueil-Malmaison, France.

Corresponding author: Z. Ouraga, zady.ouraga@ifpen.fr

Abstract
During sedimentation, buried rocks are subjected to an increase in vertical stress. This increase leads to a decrease of porosity that is commonly called mechanical compaction. Indeed, the mechanical compaction depending on its rate and on the permeability of the burden rocks, can induce significant overpressures. Thus, a competition is initiated between the dissipation of fluid overpressure and sedimentation rate, and may result in fracture initiation. The present study deals with the initiation and propagation of natural fracture in sealing formations. A particular emphasis is put on mode I fracture propagation. An analytical solution of the pressure and stresses in a sealing formation is proposed under sedimentation by superposing two problems of poroelasticity. This analytical solution and a damage criterion are used to predict the initiation and propagation of the fracture. The damage parameter affects both the mechanical and hydraulic opening of the fracture, and the flow in the fracture is described by the Poseuille's law. The fracture propagation and growth are studied by numerical simulations based on a finite element code dedicated to fractured porous media called *Porofis*. Interactions between hydraulic and mechanical processes are also studied and a sensitivity study is carried out in order to find the most important parameters involved in natural fracturing under sedimentation.

1 Introduction

Basin modeling is commonly used to describe basin's evolution from a reconstruction of its geomechanical history. It is a dynamic modeling of geological processes in sedimentary basins over geological time span [*Hantschel and Armin*, 2009]. During the geological processes modeling, the transfer properties of sediments can change significantly due to natural fracturing [*Twenhofen*, 1950; *Schneider et al.*, 1999] and therefore may constitute preferential flow paths or barrier that control hydrocarbons migration and accumulation. Thus, in petroleum industry, and especially for exploration, the knowledge of natural fracturing processes and history enhances the prediction of overpressure, potential location of hydrocarbon storage and matrix equivalent permeability. It seems obvious to observe that at depth, fractures' nucleation and initiation are triggered by existing defects, but the loads behind its initiation are unknown or poorly characterized. Fracture mechanical and geometrical properties are directly related to the processes from which it comes, and in sedimentary basin formation, fractures can appear at depth by many processes such as deposition, tectonic and erosion processes. Historically it was impossible to imagine joints initiated at very high depth which from an analytical view was inconsistent with the deep stress field. Thus, the interpretation of fracture initiation was qualitative and arose from exploitation of outcrop's database. It took until the effective stress concept introduced by *Terzaghi* [1936] and the concept of poroelasticity introduced by *Biot* [1941] to explain tensile stress at very high depth. Therefore, substantial efforts have been made to process data field and many studies began to use porous and fracture mechanics theories to better understand fracture initiation and propagation. According some of these concepts fractures initiated in the porous medium when the pore pressure exceeds the main compressive minor stress, and this phenomena is called Natural Hydraulic Fracturing [*Secor*, 1965, 1969; *Audet and McConnell*, 1992; *Mourgues et al.*, 2011; *David and Andrew*, 1990]. In fact following previous modeling [*Luo and Vasseur*, 2002; *Roberts and Num*, 1995], in some condition, the pore pressure may be locally very high compared to the minimun in situ stress and as discussed by *Secor* [1965, 1969] fracture initiated from randomly oriented small crack or flaws which are internally loaded by pore pressure in the rock mass. In this paper natural fracture initiation and propagation is studied by assuming a single phase fluid flow and the basin as a porous medium. We focus on mode I fracture initiation and propagation due to rapid sedimentation process. In fact during sedimentation, buried rock are subjected to an increase in vertical stresses which leads to a decrease of porosity. Thus, this mechanical compaction depending on the sedimentation rate and on the permeability of the burden rocks can induce significant overpressure. Therefore, a competition is initiated between the dissipation of fluid overpressure and the sedimentation rate and may result in fracture initiation. For this study fracture is represented by cohesive joint elements undergoing damage to replace the

stress intensity and toughness considerations by the normal stress and tensile stress analysis. Besides, the flow is described by the Poiseuille's law. Then, fracture initiation is studied analytically and its propagation and growth are computed by numerical simulations based on a finite element code dedicated to fractured porous media called *Porofis* [*Pouya*, 2015].

In the following basin's typical structures that are likely to produce a natural fracturing under a rapid sedimentation will be presented. Then the main governing equations of the different physical phenomena involved will be given and finally from a sensitivity study we will find the most important parameters evolved in the natural fracture propagation during sedimentation.

2 Natural fracturing in sedimentary basins

Previous studies showed that the most important mechanisms involved in natural fracturing in sedimentary basin is the fluid overpressure [*Luo and Vasseur*, 2002; *Berchenko and Detournay*, 1997; *Secor*, 1965, 1969]. In a sedimentary basin, overpressures are generally due to mechanisms such as mechanical compaction, hydrocarbon maturation or mineralogical reaction that produce additional pore pressure. Therefore, to explain the formation of some rock joint under in-situ condition *Secor* [1965, 1969] introduced the concept of natural hydraulic fracturing. As discussed by Secor, fracture is initiated by a pore pressure in the rock, when this pressure is greater than the least principal compressive stress. Then, the fracture propagation consists of many small episodes, wherein the internal fluid pressure drop in each episode (eventually stops propagation when the pressure are below the one required for propagation), and by diffusing process lead to the another propagation episode. The limit of this model is that Secor neglected pore pressure evolution in the increasing of total stress across the fracture as discussed by *Fyfe et al.* [1978]; *Gretener* [1981], and later many models have been developed. Hence *Engelder and Lacazette* [1990] proposed a model in which the driving stress for fracture initiation arises from the poroelastic behavior of the Devonian Ithaca siltstone and define some conditions likely to produce natural hydraulic fracturing. *Renshaw and Harvey* [1994] proposed a continuously propagating model by taking into account the diffusion process in the fracture.

In this paper, to study fracture initiation and propagation, a conceptual two layer model with different mechanical, hydraulic and poroelastic properties is set up. This model is constituted by a sealing formation over a highly permeable reservoir (Figure 1) and fracturing is described in an œdometric context. The œdometric context means that the vertical displacement of the basement and the horizontal displacement of the two lateral sides of this model are blocked. We assume that the vertical flow through the sealing formation does not drop

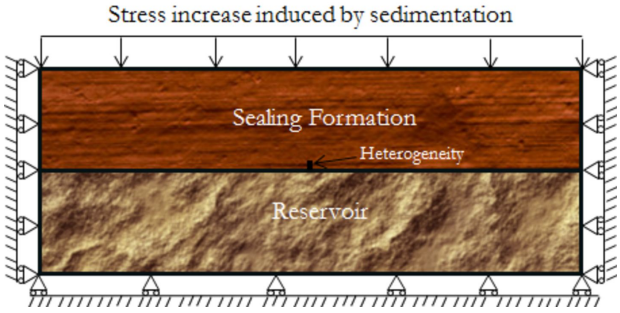

Figure 1. Two layer conceptual model and mechanical boundary conditions

significantly the amount of fluid in the reservoir. We impose a zero flux at the basement of the reservoir and the pressure at its top is considered like a reference pressure. In this framework the pressure evolution in the reservoir does not depend on its thickness (finite or infinite). Dur-

ing sedimentation process, the materials brought by water, ice and wind accumulate into the basin to form a deposit [*Lynton et al.*, 1987; *Hantschel and Armin*, 2009; *Miall*, 2000]. With time these sediments are turned into rock by diagenesis during burial. To describe the deposit of sediments it was imposed on the top of the model a vertical stress that evolves linearly with time, and a constant sedimentation rate is assumed. In this structure the contrast of mechanical and hydraulic properties between the sealing formation and the reservoir is likely to cause overpressure. The principle is that the low permeability of the seal prevents overpressure dissipation under rapid sedimentation. This phenomenon is commonly called compaction disequilibrium and is associated with potential fracturing (Bredehoef and Hanshaw, 1968; Mouchet and Mitchell, 1989; Osborne and Swarbrick, 1997; X. Luo et al., 1998). Therefore, there is a permeability depending on sedimentation rate from which significant increase of pore pressure is possible in the basin. This increase of pore pressure by hydro mechanical coupling leads to an increase of horizontal total stress in the model and with a homogeneous medium does not allow to initiate fracture. With a perturbation of pore pressure from abnormal conditions such as diagenesis, the total stress σ is generally assumed to be constant. The increase of pore pressure, leads to a decrease of the effective horizontal stress, but the total horizontal stress increases simultaneously from poroelestic relation (equation 1):

$$\sigma_h = \sigma_v \frac{\nu}{1-\nu} - bp\frac{1-2\nu}{1-\nu} \tag{1}$$

where σ_h, σ_v, ν, b are respectively the horizontal total stress, the vertical total stress, the Poisson's coefficient and the Biot's coefficient in the porous media. So, in our model to initiate opened fracture during sedimentation the overpressure generated by the contrast of properties between the sealing formation and the reservoir and the deposit of sediments are accumulated from the reservoir into the interface between the two layers in a cohesive zone (Figure 2). The presence of this more permeable zone into the sealing formation creates a local disequilibrium and can induce the initiation of fracture under certain conditions that will be analyzed in the following.

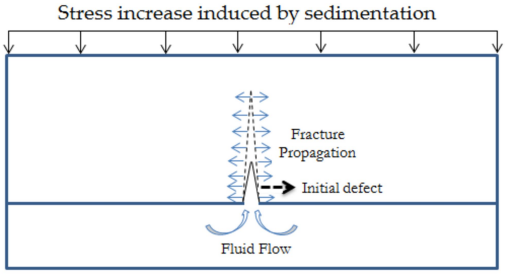

Figure 2. Mechanism to initiate fracture in the two-layer conceptual model

3 Governing equations

3.1 Flow in porous media

In this section the main equations that govern the problem of sedimentation in a porous medium are recalled [*Pouya*, 2015]. In the following we assume that the fluid is incompressible, the porous medium is isotropic the skeleton transformations are infinitesimal and the behavior of the porous material is poroelastic. We also assume that the fluid saturates the pores and the flow in the porous medium is governed by Darcy's law:

$$\underline{v} = -\frac{k}{\mu}.(\nabla p - \rho_f g) \tag{2}$$

with $\underline{v}$ the fluid velocity, p the pressure, μ the dynamic viscosity of the fluid, k the permeability and ρ_f the fluid specific mass. Without source term the mass balance equation reads:

$$div\left(\rho_f \underline{v}\right) + \frac{\partial m_f}{\partial t} = 0 \tag{3}$$

where m_f is the fluid mass per unit volume. As discussed by *Coussy* [2004] and considering our previous assumptions the governing equation describing the skeleton deformation and the motion of fluid is given by:

$$\frac{1}{M}\frac{\partial p}{\partial t} = div\left(\frac{k}{\mu}\nabla p\right) - b\frac{\partial \epsilon_v}{\partial t} \tag{4}$$

where M and b, ϵ_v represents respectively the Biot's modulus, the Biot's coefficient and the volumetric strain given by the trace of the strain tensor.

3.2 Flow in fracture

The flow in the fracture arise from fluid flow in rocks joint with a Poiseuille type law [*Guéguen and Palciauskas*, 1994; *Pouya and Ghabezloo*, 2010]. The flow q is related to the pressure gradient in the fracture surface:

$$q(s) = -C_f(s)\nabla_s p(s) \tag{5}$$

Where ∇_s is the tangent gradient in the local tangent plane to the fracture and C_f is the conductivity in the fracture. The assumption of a laminar flow between two infinite and parallel planes leads to cubic law and fracture's conductivity is linked to the fracture's hydraulic aperture e_h by:

$$C_f = \frac{e_h^3}{12\mu} \tag{6}$$

The mass balance equation in the fracture with mass exchange between fracture and matrix constitutes the main equation for the flow problem in fracture. The mass balance in a portion of the fracture between the abscises s and $s + ds$ (Figure 3) reads:

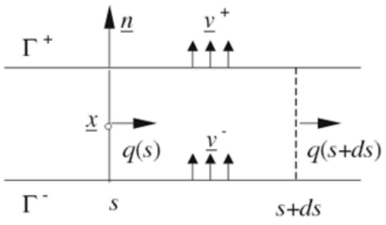

Figure 3. Masse exchange between fracture and matrix *Pouya and Ghabezloo* [2010]

$$div\left(\rho_f q\left(s\right)\right) + [\![\rho_f v\left(s\right)]\!].n\left(s\right) + \frac{\partial m_f^*}{\partial t} = 0 \tag{7}$$

where v can be discontinuous with the value v^+, v^- on the two sides of the fracture. The operator $[\![.]\!]$represents a jump across the fracture . m_f^* is the fluid mass per unit volume in the fracture and the saturation into the fracture is taken equal to 1.

$$m_f^* = \rho_f e \tag{8}$$

where e is the fracture's aperture, ρ_f is the fluid specific mass and then by differentiation :

$$\frac{\partial m_f^*}{\partial t} = \rho_f \frac{\partial e}{\partial t} + e\frac{\partial \rho_f}{\partial t} = \rho_f \frac{\partial e}{\partial t} + e\frac{\rho_f}{K_f}\frac{\partial p}{\partial t} \tag{9}$$

where K_f is the fluid compressibility. By combining the equation (5, 9), and simplification the equation (7) leads to :

$$div\left(c_f \nabla_s p\right) = \frac{e}{K_f}\frac{\partial p}{\partial t} + [\![v]\!].n + \frac{\partial e}{\partial t} \tag{10}$$

3.3 Hydro mechanical coupling

Hydromechanical coupling represents the interaction between mechanical and hydraulic processes [*Neuzil*, 2003; *Rutqvist and Stephansson*, 2003]. Total stress applied into the porous media is the sum of the load applied on skeleton and the load applied on fluid. Generally the total stress is given by:

$$\underline{\underline{\sigma}} = \underline{\underline{\underline{\underline{C}}}} : \underline{\underline{\epsilon}} - bp\underline{\underline{I}} \tag{11}$$

The sign convention of continuum mechanics is used, stress and strain are positive in tension. $\underline{\underline{\underline{\underline{C}}}}$ represents the elasticity tensor, and b is the Biot's coefficient. In our model the transition from mechanical computation to hydraulic occurs when the variation of applied stress or fracture opening induces a significant pore volume change and thereby, potentially, a significant change in the pore pressure or in the fluid mass. The transition from hydraulic computation to mechanics occurs when the pressure or mass fluid variation into porous media is high enough to lead to a significant change in volume or in the opening of fractures. The coupling between mechanical and hydraulic problems is performed with a sequential solving of the two problems and iteration between them. The sequential solving used here, consists in solving the flow problem first through considering constant the total mean stress field. Once the flow problem is computed , the mechanical problem is solved and the volumetric strain term $b\frac{\partial \epsilon_v}{\partial t}$ in the equation (4) is computed explicitly [*Kim et al.*, 2010; *Guy et al.*, 2012a]. this resolution show stability for both elasticity and elastoplasticity and can be applied safely to poromechanical problem [*Kim et al.*, 2010] such as to modeling the hydromechanical behavior of reservoir during production [*Longuemare et al.*, 2002] or fracture propagation during sedimentation.

3.4 Description of cohesive zone model with damage

The numerical simulations are based on the cohesive zone model proposed by *Pouya and Bemani* [2015]. The particularity of this model is that it describes the evolution of fracture cohesion, tensile strength and elastic stiffness with damage under combined shear and normal stress loads. It is an extension of the model proposed by *Carol et al.* [1997] and the elasticity-damage coupling is given by:

$$\underline{\sigma_J} = (1 - D)\,\underline{\underline{k}}\,\underline{u} \tag{12}$$

where $\underline{\sigma_J}$, D, $\underline{\underline{k}}$, are respectively the stress tensor in the joint, the damage variable in the fracture, and the joint stiffness tensor. The vector is the relative displacement, and represents the jump of discontinuity between the two side of the fracture. Experiments conducted on a large number of samples show that normal displacements under normal stress are nonlinear with a maximum closure which is interpreted as the physical thickness of joint [*Bandis et al.*, 1983]. However *Bandis et al.* [1983] formulation doesn't distinguish loading and unloading paths and doesn't include the progressive stiffness degradation due to opening of rock joints. Pouya and Bemani take into account the gradual rock joints stiffness degradation by a scalar variable D which affect stiffness due to rock joint and the loading paths. In this paper, we extend their model to porous context and under shear and normal stress this model leads to:

$$\tau + bp = (1 - D)\,k_{tp}u_t^e = k_{tD}u_t^e \tag{13}$$

$$\sigma_n + bp = (1 - D)\,k_{np}u_n^e = k_{nD}u_n^e, \quad u_n^e \geq 0 \tag{14}$$

$$\sigma_n + bp = (1 - D)\,k_{np}u_n^e - \frac{k_{nf}\left(u_n^e\right)^2}{e_{max} + u_n^e} = k_{nD}u_n^e, \quad u_n^e \prec 0 \tag{15}$$

where σ_n, τ, u_t^e, u_n^e are respectively the normal and shear stress and the elastic relative tangential and normal displacement in the joint. The parameter k_{nD} and k_{tD} are the equivalent

normal and shear stiffness to take into account the damage effect in the joint. The stiffness indexed by tp appears in shear load and the one indexed by np is in compression as well as in tensile stress and disappear at the ultimate damage state. Under compression an another term occurs and doesn't depend on the joint damage. This term has a hyperbolic shape and is a function of the maximum closure e_{max} of the joint and the stiffness indexed by nf represents rock joint stiffness during the closure stage [*Pouya and Bemani*, 2015]. The evolution of criterion of the damage D depends on the relative elastic displacement limit of the cohesive fracture u_0. Under a displacement u_0 the damage D remains equal to zero and increases exponentially with the normal joint displacement u_n:

$$D = 1 - e^{-\frac{(u_n - u_0)}{\beta u_0}}, u_n \geq u_0 \tag{16}$$

where β characterizes material ductility and varies in $[0, \infty[$. High β represents a ductile material on the contrary $\beta = 0$ represents a brittle material. The cohesive joint behavior is plotted on Figure 4 for different values β. The failure criterion depends on damage and is

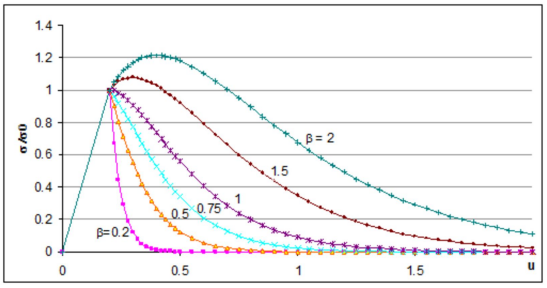

Figure 4. Normalized stress versus displacement in the cohesive zone model [*Pouya and Bemani*, 2015]

defined as followed (Figure 5):

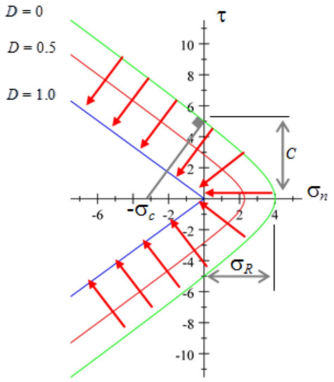

Figure 5. Evolution of the failure criterion from intact rock joint to the final damage rock joint [*Pouya and Bemani*, 2015]

$$F(\tau, \sigma_n, D) = \tau^2 - \sigma_n^2 tan^2\varphi + 2g(D)\,\sigma_c \sigma n - g^2(D)\,C^2 \tag{17}$$

where C represents the cohesion on intact cohesive fracture, τ and σ_n are the tangential and normal stresses and φ is the friction angle and :

$$\sigma_c = \frac{C^2 + \sigma_R^2 tan^2\varphi}{2\,\sigma_R} \tag{18}$$

with σ_R the limit tensile strength of the intact joints. The function $g(D)$ is obtained by using consistency condition and it is given by:

$$g(D) = (1 - D)(1 - \beta ln(1 - D)) \tag{19}$$

for an intact rock $D = 0$ and $g(D) = 1$ and for completely damage fracture $D = 1$ and $g(D) = 0$.

4 Fracture initiation condition

4.1 Conceptual model

The fracture initiation is studied analytically from a model equivalent to the basic model (Figure 1). Given that the study is focused on the initiation of opened fracture under rapid sedimentation on the sealing formation, only this layer is modeled in the following. In fact, the pore pressure evolution considered for the reservoir is applied as a boundary condition at the basement of the seal. Considering that the permeability of the sealing formation is very

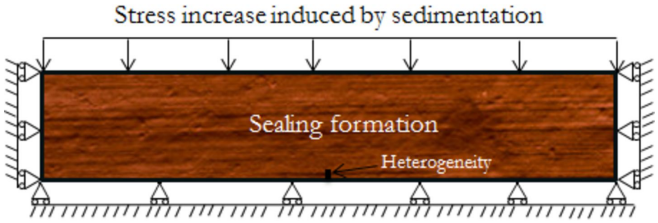

Figure 6. Conceptual model for fracture initiation study and mechanical boundary conditions; the pressure evolution in the reservoir of the basic model is imposed as a boundary condition at the basement of this model

smaller than the permeability of the reservoir, we can assume that, at the considered time scale, the flow from reservoir to the sealing formation is low enough to represent a neglectable part of the amount of fluid in the reservoir. The reservoir evolution can thus be considered to an undrained deformation. In this case, as discussed by *Coussy* [2004] (section 4.3.2), the fluid mass changes leads to:

$$\frac{dm_f}{\rho_f} = bd\epsilon_v + \frac{dp}{M} \tag{20}$$

with the undrained behavior of the reservoir, the fluid mass changes are prevented ($dm_f = 0$) and the equation 20 becomes:

$$dp = -bMd\epsilon_v. \tag{21}$$

From equation (11), and the hypothesis of a linear isotropic poroelastic skeleton the total stress in the reservoir is given by Hooke's law:

$$\sigma_{ij} = \left(K_r - \frac{2}{3}G_r\right)\epsilon_{kk}\delta_{ij} + 2G_r\epsilon_{ij} - bp\delta_{ij} \tag{22}$$

where K_r is the bulk modulus of the reservoir and G_r its shear moduli. With the oedometric boundary condition and equation 22, the volumetric strain variation leads to:

$$d\epsilon_v = \frac{d\sigma_v}{\frac{3(1-\nu_r)K_r}{(1+\nu_r)}} + \frac{bdp}{\frac{3(1-\nu_r)K_r}{(1+\nu_r)}} \tag{23}$$

and the equation 20 becomes:

$$dp = \frac{-bd\sigma_v}{\frac{3(1-\nu_r)K_r}{M(1+\nu_r)} + b^2}. \tag{24}$$

Given that σ_v the vertical applied loading is a linear function of time, the pressure evolution in the reservoir is also a linear function of time and by integration the equation 24 becomes:

$$p(t) = \frac{-b}{\frac{3(1-\nu_r)K_r}{M(1+\nu_r)} + b^2}\sigma_v. \tag{25}$$

The equation 25 gives the pressure evolution in the reservoir that will be imposed as boundary condition at the basement of the seal formation. The fracture initiation condition will be based on the analytical solution of pore pressure and stress evolution in space and in time in a homogeneous porous medium with same boundary conditions that the equivalent conceptual model (Figure 6). The principle is to analyze local hydro-mechanical condition of non-equilibrium due to the presence of a defect, likely to gather favorable condition to initiate fracture from the failure criterion.

4.2 Closed form solution

The diffusion problem in the homogeneous porous medium to solve is presented in the Figure 7 below. In this problem, there are two time dependent mechanisms involved. First,

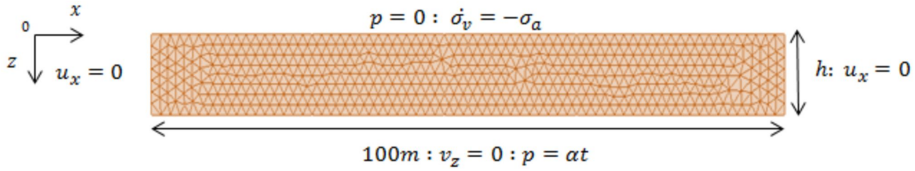

Figure 7. Homogeneous model and boundary condition, $\alpha = \frac{b}{\frac{3(1-\nu_r)K_r}{M(1+\nu_r)}+b^2}\sigma_a$

the deposit of sediment during sedimentation process taken into account with a constant sedimentation rate $\dot{\sigma_v} = -\sigma_a$ and second the pore pressure evolution in the reservoir depending on this loading during time is given by equation 25. To solve this problem given that a poroelastic behavior of the model a superposition principle of the two mechanisms is applied. The problem is divided into two sub-problems complying with hydraulic and mechanical boundary conditions and equilibrium conditions. The first sub-problem consists in a consolidation case with a source term (Figure 8) and, unlike the equivalent basic model, a zero pressure is imposed at its basement. In the second sub-problem a zero sedimentation rate is assumed and a pressure that evolves with time is imposed at the basement (Figure 9).

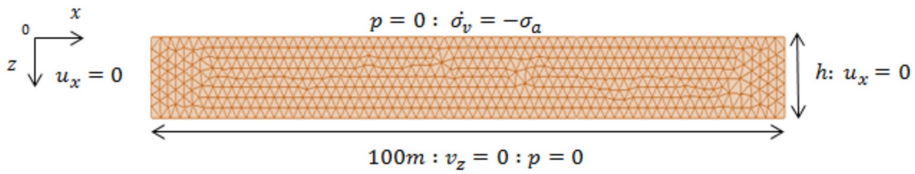

Figure 8. Geometry and boundary conditions of sub-problem 1

The sub-problem 1 is equivalent to a problem of a slab with heat produced within it as discussed by *Carslaw and Jaerger* [1959]. In the sub-problem 1 the governing equation

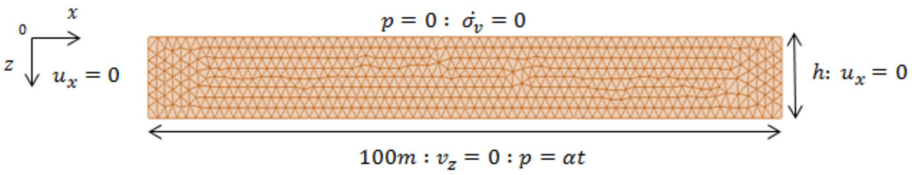

Figure 9. Geometry and boundary conditions of sub-problem 2

describing the skeleton deformation and the fluid flow results from equation 4 and leads to:

$$\left(\frac{1}{M} + \frac{3(1+\nu)b^2}{(1-\nu)K_s}\right)\frac{\partial p(z,t)}{\partial t} - \frac{3(1+\nu)b}{(1-\nu)K_s}\sigma_a = \frac{k}{\mu}\frac{\partial^2 p(z,t)}{\partial^2 z}. \tag{26}$$

From equation 26, boundary conditions and initial conditions $t = 0,\ p(z,0) = 0$, the pressure evolution of the sub-problem over time and in space is given by:

$$p_1(z,t) = \frac{-3\mu(1+\nu)b}{2k(1-\nu)K_s}\sigma_a\left(z^2 - zh\right) - \frac{12\mu b(1+\nu)b\sigma_a h^2}{k(1-\nu)K} \times \sum_{n=0}^{\infty}\frac{1}{\pi^3(2n+1)^3}\sin\left(\frac{(2n+1)\pi z}{h}\right)e^{-\left(\frac{(2n+1)^2\pi^2}{h^2}\tau_s t\right)} \tag{27}$$

where $\tau_s = \frac{k}{\mu\left(\frac{1}{M} + \frac{3(1+\nu)b^2}{(1-\nu)K_s}\right)}$ represents the fluid diffusivity coefficient in the sealing formation as discussed by *Coussy* [2004], K_s the seal bulk modulus, M the Biot's modulus , and k the permeability.

The pressure evolution over time and in space of the sub-problem 2 is given by equation 28 below:

$$\frac{\partial p(z,t)}{\partial t} = \tau_s\frac{\partial^2 p(z,t)}{\partial^2 z}. \tag{28}$$

To solve equation this equation with boundary conditions changing with time, let us introduce the auxiliary function $p_\infty(z,t)$ given by:

$$p_\infty(z,t) = \frac{\alpha}{6\tau_s h}\left(z^3 - zh^2\right) + \frac{\alpha t}{h}z \tag{29}$$

This function satisfies the same equation (28) and has the following limit property:

$$\lim_{t\to+\infty}\frac{\partial p_\infty(z,t)}{\partial t} = \frac{\alpha z}{h} \tag{30}$$

If we introduced the new unknown $\theta(z,t)$ defined by:

$$\theta(z,t) = p(z,t) - p_\infty(z,t) \tag{31}$$

then, $\theta(z,t)$ satisfies:

$$\frac{\partial\theta(z,t)}{\partial t} = \tau_s\frac{\partial^2\theta(z,t)}{\partial^2 z} \tag{32}$$

with the boundary conditions:

$$\begin{cases} z = 0, & \theta(0,t) = 0 \\ z = h, & \theta(h,t) = 0 \\ t = 0, & \theta(z,t) = -p_\infty(z,0) \end{cases} \tag{33}$$

A general form of the function $\theta(z,t)$ is obtained as an infinite sum of function:

$$\theta(z,t) = \sum_{n=0}^{\infty}A_n\sin\left(\frac{n\pi}{h}z\right)e^{-\left(\frac{n^2\pi^2}{h^2}\tau_s t\right)},$$
$$A_n = \frac{2}{h}\int_0^h -p_\infty(z,t)\sin\left(\frac{n\pi}{h}z\right)dz. \tag{34}$$

Integrating A_n, leads to:

$$\theta(z,t) = \frac{-2\alpha h^2}{\tau_s} \sum_{n=1}^{\infty} \frac{1}{\pi^3 n^3} \sin\left(\frac{n\pi}{h} z\right) e^{-\left(\frac{n^2\pi^2}{h^2}\tau_s t\right)}. \tag{35}$$

From equation 31 the pressure evolution evolution of the sub-problem 2 over time and in the space reads:

$$p_2(z,t) = \frac{\alpha}{6\tau_s h}\left(z^3 - zh^2\right) + \frac{\alpha t}{h} z - \frac{2\alpha h^2}{\tau_s} \sum_{n=1}^{\infty} \frac{(-1)^n}{\pi n}\left(\frac{1}{\pi^2 n^2} - \frac{\tau_s t}{h^2}\right) \sin\left(\frac{n\pi}{h} z\right) e^{-\left(\frac{n^2\pi^2}{h^2}\tau_s t\right)} \tag{36}$$

With the superposition principle, the horizontal stress evolution over time and space is given by equation 1 and the pressure evolution over time and space in the homogeneous model is the sum of the pressure evolution of each sub-problem (equation 27, 36):

$$p(z,t) = \frac{\alpha}{6\tau_s h}\left(z^3 - zh^2\right) + \frac{\alpha t}{h} z - \frac{2\alpha h^2}{\tau_s} \sum_{n=1}^{\infty} \frac{(-1)^n}{\pi n}\left(\frac{1}{\pi^2 n^2} - \frac{\tau_s t}{h^2}\right) \sin\left(\frac{n\pi}{h} z\right) e^{-\left(\frac{n^2\pi^2}{h^2}\tau_s t\right)} -$$
$$\frac{3\mu(1+\nu)b}{2k(1-\nu)K_s}\sigma_a\left(z^2 - zh\right) - \frac{12\mu b(1+\nu)b\sigma_a h^2}{k(1-\nu)K_s} \sum_{n=0}^{\infty} \frac{1}{\pi^3(2n+1)^3} \sin\left(\frac{(2n+1)\pi z}{h}\right) e^{-\left(\frac{(2n+1)^2\pi^2}{h^2}\tau_s t\right)}. \tag{37}$$

4.3 Analysis of fracture initiation

The analysis of fracture initiation will be based on the analytical pressure evolution over time and space described above. To initiate fracture, an initial hydraulic defect is introduced in the model (Figure 6). This defect is a cohesive zone wherein the permeability is greater than the permeability of the surrounding media. According to our failure criterion (equation 17), for a mode I propagation ($\tau = 0$), the facture initiates when the normal effective stress in the cohesive zone reaches σ_R. In the basin context and for a vertical opening fracture, the fracture onset corresponds to:

$$\sigma_h + b_f p_p = \sigma_R \tag{38}$$

where σ_h is the horizontal total stress, b_f the Biot's coefficient of the cohesive joint equal to the unity in this study, σ_R the limit tensile strength of the porous medium and p_p the pore pressure. We recover by this way the failure criterion established in previous studies [*Sibson*, 2003; *Cosgrove*, 2001; *Rozhko et al.*, 2007]. To characterize fracture initiation condition in the porous media a sensitivity study is done in the following (Figure 10). The aim is to analyze the influence of the main parameters involved in fracturing process under sedimentation. During sedimentation, many flaws of centimeter to metric length can be incrusted at the interface between the sealing formation and the reservoir that locally enhance the conductivity of the rock. As seen in figure 10(a), (b), the normal effective stress in this defect can reach a maximum tensile stress after a certain period of time and then decrease to become compressive. Results plotted in figure 10 (a), (b) arose from the evolution of normal effective stress at the tip of a hydraulic defect of $0.2\ m$ and $0.02\ m$ for several sedimentation rate (10 (a)) and for several intrinsic permeability (10 (b)). these figures show that the maximum tensile stress depends on the sedimentation rate and the permeability of the sealing formation. As an example, according to our results for a relatively rapid sedimentation rate $200\ m/Myrs$ and an intrinsic permeability k from $10^{-17}\ m^2$ to $10^{-22}\ m^2$, fracture can be initiated with an initial hydraulic defect of $0.02\ m$ with a tensile strength σ_R, which is very close to zero for the case of $10^{-17}\ m^2$ and lower than $3\ MPa$ for the case of $10^{-22}\ m^2$ (figure 10 (a), (b)). In figure 10 (c), we plot the evolution of hydraulic defect length for several sedimentation rate with the parameter κ. In fact the parameter κ represents the ratio of the increasing rate of pressure in the reservoir to the increasing rate of stress due to sedimentation. The curves in figure 10 (c) are obtained with a tensile strength of the medium $\sigma_R = 200\ KPa$. In this figure, The more κ is small, the more the hydraulic heterogeneity required to initiate fracture is high. On the contrary when κ is close to the unity, fractures can initiate with small heterogeneity even though there is a low sedimentation rate (figure 10 (c)) for intrinsic permeability lower than $10^{-20}\ m^2$

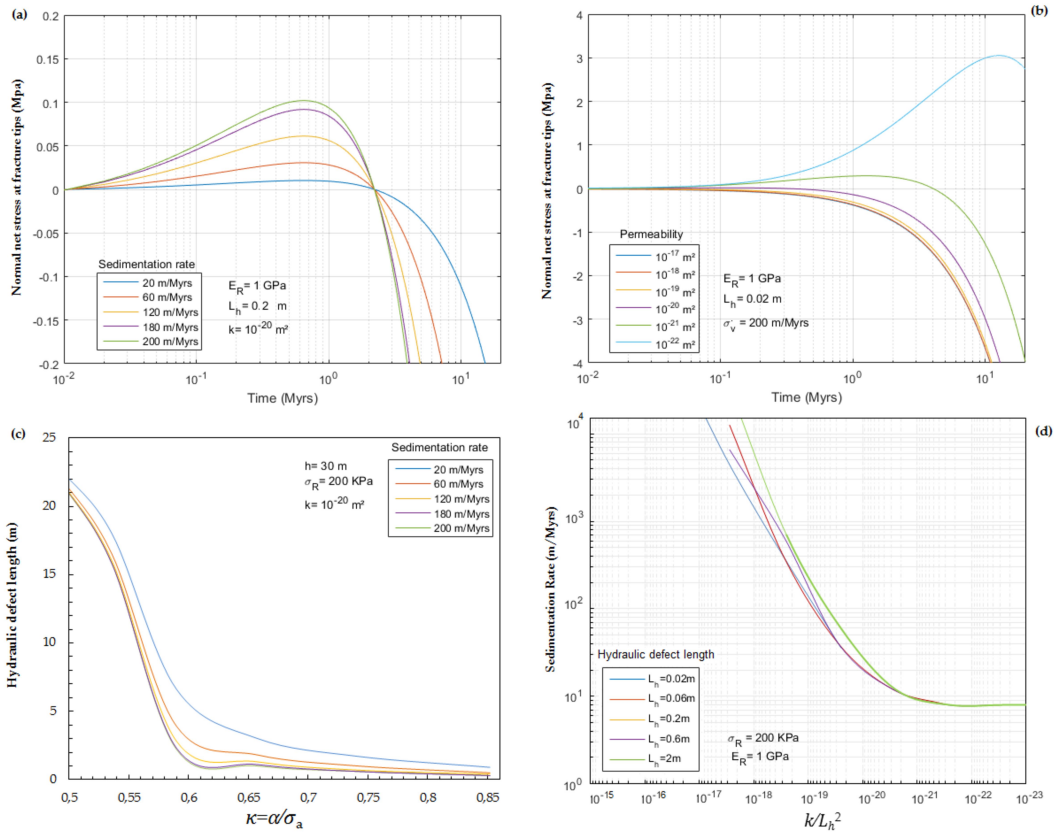

Figure 10. Evolution of normal net stress at fracture tips versus time for several sedimentation rates (a) and several intrinsic permeability (b), (c) evolution of hydraulic defect versus the ratio between the increasing rate of pressure in the reservoir and the increasing rate of stress due to sedimentation, (d) evolution of sedimentation rate versus ratio of intrinsic permeability to defect's length for several hydraulic defect

with a tensile strength $\sigma_R = 200\ KPa$. Thus, to study the influence of permeability and defect's length on fracture onset, in figure 10 (d) we plot for a given hydraulic heterogeneity, the critical sedimentation rate to initiate fracture in the medium versus the ratio of intrinsic permeability to the square of the defect length with a tensile strength of $\sigma_R = 200\ KPa$. As seen in this figure all curves of evolution of critical sedimentation rate almost collapse into the same curve. It gives ranges of sufficient sedimentation rates to initiate fractures knowing the length of heterogeneity in the past in the porous medium. It also shows that this critical deposition rate does not depend much on the defect's length but on the parameter k/L_h^2 . Therefore, a defect of centimeter range which may be frequent in the porous formations, require a very low permeability to initiate and then propagate. From this sensitivity study we have found two important dimensionless parameters κ and k/L_h^2, involved in fracture initiation under sedimentation. All of this analysis has been made with a ratio of Young's modulus of the seal to the Young's modulus of the reservoir equal to 3 because the length of the heterogeneity does not vary significantly when this ratio is greater than unity for a fixed κ (see figure 11, $\kappa = 0.85$). Results of this sensitivity study will be used in the following for the numerical modeling.

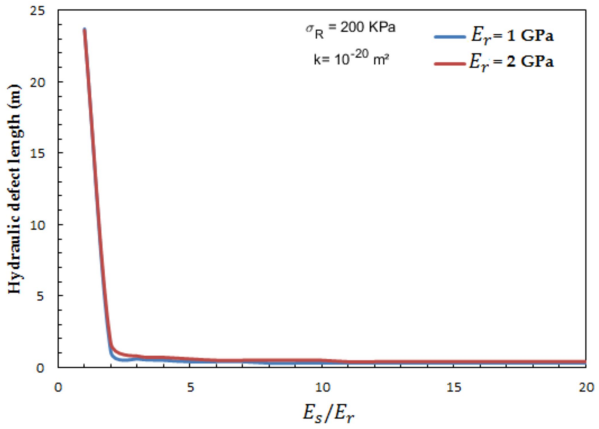

Figure 11. Evolution of hydraulic defect length versus the ratio of Young's modulus of the seal formation and the reservoir

5 Modeling of fracture propagation

5.1 Numerical modeling

In this section the numerical modeling of the equivalent two-layer model is presented (Figure 12).

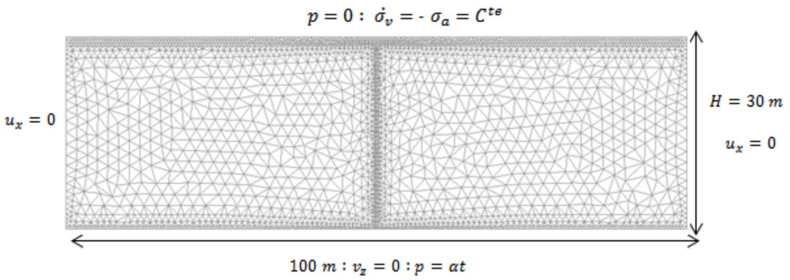

Figure 12. FEM numerical simulation model with single fracture

The seal formation has a height of $30\ m$ and the model extends over a length of $100\ m$. A predetermined cohesive zone is introduced in this formation over its entire height and the potential fracture is assumed to be vertical; it can be considered as a relevant hypothesis as an example in a situation of low horizontal total stress to vertical stress ratio [*Guy et al.*, 2010, 2012b]. Fracture in the seal is divided into two parts. The first part consists in the hydraulic defect. It is around $0.6\ m$ length and is very permeable with a parameter $\lambda = C_t/2kL \geq 100$ (C_t, k, L respectively are the fracture's conductivity, matrix permeability and fracture's length). As discussed by *Pouya* [2015], pressure is constant along the fracture with λ greater than 100 and in our case this pressure is equal to the pressure in the reservoir. In the second part of the fracture, the parameter λ is closed to zero which means that the fracture is inexisting for a hydraulic computation.

For the mechanical problem the node on the cohesive joint is splitted to allow displacement discontinuities across fracture while for the hydraulic problem it is not necessary because the pressure in our case is the same on the two sides of the fracture. On each side of the fracture, the displacement and the pressure of node are the same that in the matrix. The continuity of the pressure at matrix/fracture interface with the equation (10) ensure the mass balance

equation as explained by [*Pouya*, 2012].To account for continuous degradation of fracture mechanical properties and its impact on hydraulic computation, it assumes that hydraulic opening is connected to mechanical opening given by equation (14), by the scalar D that represents fracture damage. Mechanic and hydraulic parameters are chosen such that the initial fracture has no mechanical influence on numerical simulation until its initiation. It also assumes an initial hydraulic opening e_{h0}, associated with the conductivity C_{t0} close to zero and an initial storage coefficient of fracture S_{f0}. During the numerical simulation we define the hydraulic opening e_h for a given normal stress in the cohesive zone by :

$$e_h = e_{h0} + \langle u_n^e \mid_D - u_n^e \mid_{D=0} \rangle \quad (39)$$

where in this expression, for example $\langle x \rangle$ represents the positive part of x, i.e $\langle x \rangle = \frac{x+|x|}{2}$. Let $e_m = u_n^e$ be the mechanical opening of the cohesive zone. From equation 14, the equation 39 becomes:

$$e_h = e_{h0} + \langle e_m - (1-D)\, e_m \rangle = e_{h0} + D \langle e_m \rangle \quad (40)$$

with the hydraulic opening e_h, the fracture's conductivity during the simulation is given by the cubic law:

$$\begin{cases} C_t = C_{t0} \times \left(\frac{e_h}{e_{h0}}\right)^3 \\ S_f = S_{f0} \times \left(\frac{e_h}{e_{h0}}\right) \end{cases} \quad (41)$$

where C_t, S_f are respectively the conductivity of the fracture and its storage coefficient. Under these formulations fracture propagates by continuous fracture damage and the failure and damage criterion control the fracture propagation.

5.2 Simulation results

The parameters shown in Table 1 are used for numerical fracture initiation and propagation modeling ($\kappa = 0.85$ and $\frac{E_s}{E_r} = 3$). These parameters are realistic comparating of data of poroelastic constant for water saturated rocks [*Detourney et al.*, 1987; *Atkinson and Meredith*, 1987; *Touloukian et al.*, 1989].

Table 1. Input data for simulation

Property	Seal Formation	Reservoir
Permeability (matrix)	$10^{-20}\ m^2$	$10^{-12}\ m^2$
Young Modulus (matrix)	3 GPa	1 GPa
Poisson ration	0.23	0.2
Biot coefficient	1	1
Overburden	200 m/Myrs	

Analysis of FEM results show that fracture initiate when the cohesive joint begins to damage about $0.6\ Myrs$ after load application and its normal effective stress reaches the limit tensile strength of the seal formation $\sigma_R = 0.2\ MPa$ (see Figure 13, Figure 14). The Figure 14 shows a good agreement between the previous initiation study and the numerical result and also the constitutive law of the cohesive joint. Indeed, after damage, when the scalar D is closed to the unity the normal stress stay, close to zero. Fracture propagation is related to damage evolution and to the cohesive joint opening. After initiation, the fracture propagates with a staggered evolution. The stress at the fracture tips must first reach the failure criterion and then cause a damage increase in the cohesive joint in oder to make it propagate. Each joint element has a length of about $0.1\ m$. The first joint damages at about $0.6\ Myrs$ after load application that corresponds the fast sedimentation process and then propagates up to its entire length in approximately $0.58\ Myrs$. The damage law is given by equation 16 when the opening exceeds the value u_0. In our numerical simulation $\beta = 1$ corresponds to a low

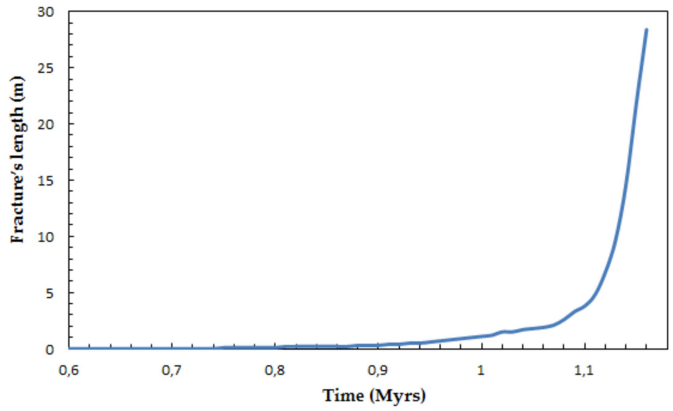

Figure 13. Fracture's length evolution versus time

ductility material. After $1.11\ Myrs$ the fracture length is only about $5\ m$ and from this time it propagates quickly and extends in less than $0.1\ Myrs$ throughout all the model's height. The

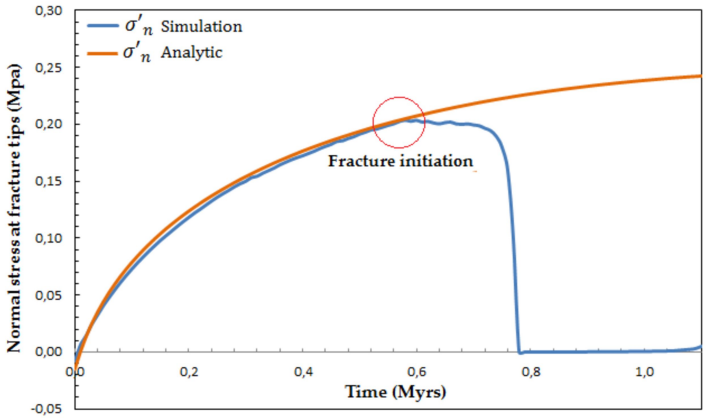

Figure 14. Analytical and numerical evolution of the normal stress at the hydraulic defect tips

fracture propagation during the simulation is plotted in Figure 15. The flow is initially focused on the permeable part of the joint corresponding to the lowest $0.6\ m$ and then propagates when the criterion failure is reached. After initiation, the fracture propagation depends on the competition between the fluid dissipation and the loading speed. Simulation with the same parameters but different loading speed has shown that in some cases fracture can initiate but not propagate as seen in Figure 16. The blue, and red curves represent the evolution of fracture length and the normal stress at the fracture tip respectively under a sedimentation rate of $200\ m/Myrs$, and $160\ m/Myrs$.

The analysis of Figure 16 shows the impact of sedimentation rate on fracture propagation. Indeed, the higher is the sedimentation rate, the higher is the probability to have fracturing in low permeability layers. In some cases, as the one associated with the red curve, fracture can initiate at the interface between the two layers without propagating significantly.

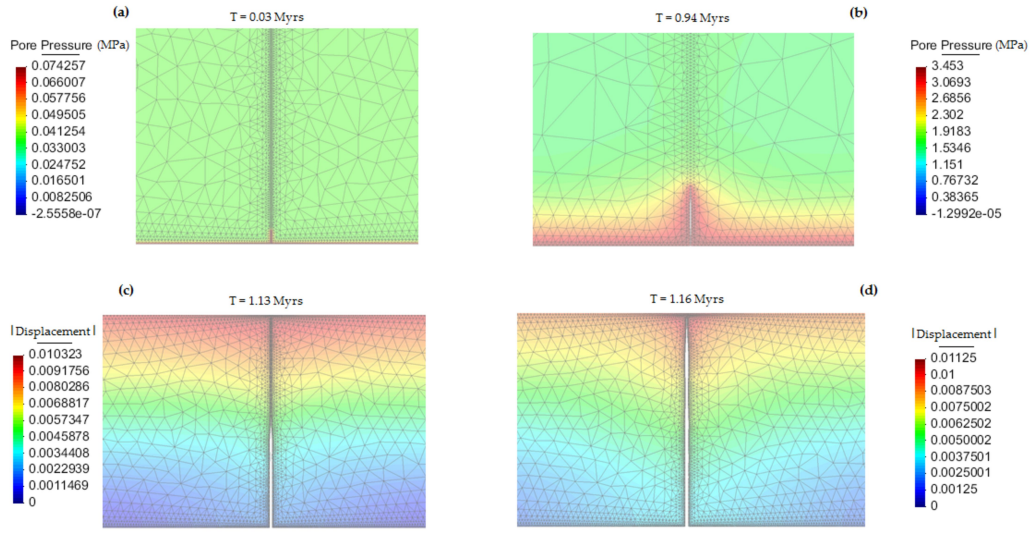

Figure 15. Simulation results of fracture propagation and pressure evolution (a,b) and the norm of the displacement (c,d)

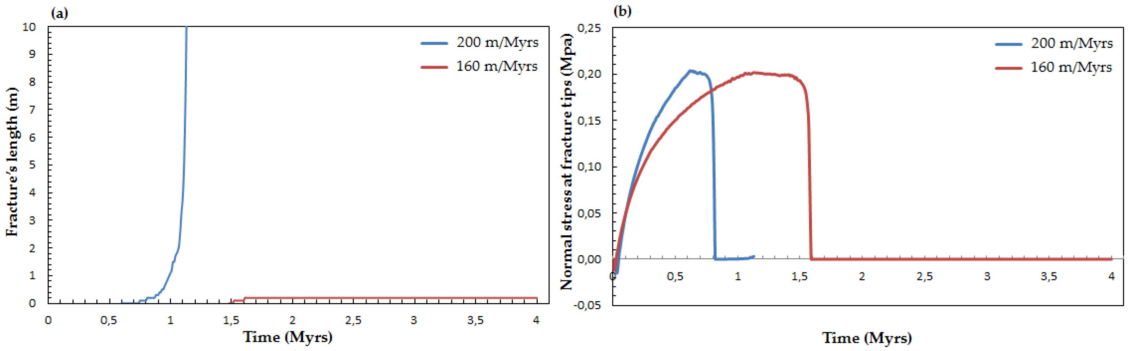

Figure 16. Evolution of the fracture and stress at fracture tips for 200 m/Myrs and 160 m/Myrs

6 Discussion and Conclusion

In this study, fracture propagation under rapid sedimentation has been analyzed. The time duration considered for simulation is smaller than the characteristic diffusion time in the seal and the hydraulic defect. To study fracturing process from initiation until the propagation in the seal, a model with a predetermined fracture propagation path has been set. *Renshaw and Harvey* [1994] pointed out that natural fracturing takes place from initial defects in the material and hence from its heterogeneity. Moreover, to describe initiation of fracture in different contexts many authors [*Weibull*, 1939; *Hild*, 2001; *Turcotte and Glasscoe*, 2004] consider a method based on the relation between heterogeneity of the media and the failure probability. The idea of this approach is to describe the heterogeneity of the media by a distribution of load level generating fractures. Based on these ideas we have studied fracture initiation by introducing a heterogeneity called hydraulic defect. Initiation analysis consisted in an evaluation of the impact of the heterogeneity on pressure field and on effective stress. This study has been a criterion to define heterogeneity's length required to initiate fracture propagation, for given hydraulic and mechanical properties of the seal and the reservoir. The hydraulic defect was taken into account by assuming a cohesive zone near the interface between the seal and the reservoir layers (very small compared to the height of the model). This zone is more permeable than the seal with properties corresponding to a compacted clay sediment. To characterize

fracture initiation and to evaluate the influence of Young's modulus of the reservoir, the seal's permeability, and the ratio between the increasing rate of pressure in the reservoir and the increasing rate of stress due to sedimentation, a parametric study was performed based on an original analytical solution (equation 37). Whereas numerical simulation is used to describe the propagation, this analytical solution allows to study fracture initiation in single phase fluid flow. For the case of an unsaturated fracture a two-phase flow in cracks or fractures a generalized effective stress could be used [*Rozhko*, 2016]. Our analytical solution helps to identify the most important variables affecting fracture propagation during sedimentation and to better understand the conditions of natural fracturing process. Thereby with our analysis we have shown that the critical length of heterogeneity necessary for triggering fracture propagation depends on the ratio between the increasing rate of pressure in the reservoir and the increasing rate of stress due to sedimentation, but also on the permeability of the medium and the ratio between the Young's modulus of the seal formation and the reservoir. Indeed, when the seal formation is stiffer than the reservoir, parameters involved to initiate fracture are κ (which represents the ratio between the increasing rate of pressure in the reservoir and the increasing rate of stress due to sedimentation) and the permeability. By contrast, when the reservoir is stiffer than the seal, the overpressure in the reservoir is not enough to lead natural hydraulic fracturing with flaws of about centimeter to meter range without other contributions such as tectonics or erosion. Our numerical and initiation study are in conformity with the observations of [*Engelder and Lacazette*, 1990] in the Devonian Ithaca siltstone near Watkins Glen, New York. By using fracture mechanic *Engelder and Lacazette* [1990] show that fracture is initiated when pore pressure are around 85% of the overburden stress and at flaw locations of about $1 - 3\ cm$ diameters (such as fossils, concretions or flute casts). By analogy, we have shown that the higher is κ (which represents the ratio between the increasing rate of pressure in the reservoir and the increasing rate of stress due to sedimentation), the higher is the possibility to gather favorable conditions to initiate fracture at the interface between the two layers. For example, with a $\kappa = 0.85$, according to our study a fracture can initiate with a small heterogeneity around $2\ cm$ with a relatively rapid sedimentation rate $200\ m/Myrs$ and intrinsic permeability from $10^{-19}\ m^2$ to $10^{-22}\ m^2$. We have also found that the critical sedimentation rate to fracture onset does not depend only on the defect's length but more on the parameter k/L_h^2. Finally, the fracturing criterion presented in this paper can be considered to model natural hydraulic fracturing under rapid sedimentation in a realistic context.

Acknowledgments

This work was funded by an IFP Energies Nouvelles research program. I would like to thank the anonymous reviewers for their interesting comments that improve the quality of this work. The data for this paper are available by contacting the corresponding author at zady.ouraga@ifpen.fr.

References

Atkinson, B. K., and P. G. Meredith (1987), Experimental fracture mechanics data for rocks and mineral, *Fracture Mechanics of Rock*, *San Diego, Calif*, 477–525.

Audet, D., and J. McConnell (1992), Forward modmodel of porosity and pore pressure evolution in sedimentary basins, *Basin research*, *4, No 2*, 147–162.

Bandis, S., A. Lumsdem, and N. Barton (1983), Fundamentals of rocks joint deformation, *International Journal of Rock mining science and Geomechanic*, *4, No 6*, 249–268.

Berchenko, I., and N. Detournay, E. Chandler (1997), Propagation of natural hydraulic fractures, *International Journal of Rock mechanic and Minning*, *34, No 3-4*, Paper No. 063.

Biot, M. (1941), General theory of three-dimensional consolidation, *Journal of Applied Physics*, *12*, 155–164.

Carol, I., P. Prat, and L. C.M (1997), Normal/shear cracking model: application to discrete crack analysis, *Journal of Engineering Mechanics*, *123(8)*, 765–773.

Carslaw, H., and J. Jaerger (1959), *Conduction of heat in solids*, Oxford at the Clarendon Press.

Cosgrove, J. a. (2001), Hydraulic fracturing during the formation and deformation of a basin : a factor in the dewatering of low-permeability sediments., *AAPG Bulletin*, *85(4)*, 737–748.

Coussy, O. (2004), *Poromechanics*, John Wiley & Son Ltd.

David, M. M., and S. Andrew (1990), Prediction of pore pressures in sedimentary basins, *Marine and Petroleum Geology*, *7*, 55–65.

Detourney, E. J., J. Roegiers, and A. D. Cheng (1987), Some new examples of poroelastic effects in rock mechanics, in *Proceedings of the 28th U.S. Symposium of Rock Mechanics. University of Nevada Press, Reno, Nevada, pp575-584*.

Engelder, T., and A. Lacazette (1990), *Natural hydraulic fracturing*, Rock Joints.

Fyfe, W., N. Price, and A. Thompson (1978), *Fluids in the Earth's Crust*, Elsevier.

Gretener, P. (1981), *Pore pressure : Fundamentals, general ramifications and implications for structural geology*, American Association of Petroleum Geologist Educational Course Note Serie No 4.

Guéguen, Y., Y.guen, and V. Palciauskas (1994), *Introduction to Physics of Rocks*, Princeton University Press.

Guy, N., D. Seyedi, and F. Hild (2010), Hydro-mechanical modmodel of geological co2 storage and the study of possible caprock fracture mechanisms, *Georisk*, *4(3)*, 110–117.

Guy, N., G. Enchery, and R. G (2012a), Numerical modeling of thermal eor: comprehensive coupling of an amr-based model of thermal fluid flow and gepmechanics, *Oil*, *67(6)*, 1019–1027.

Guy, N., D. Seyedi, and F. Hild (2012b), A probabilistic nonlocal model for crack initiation and propagation in heterogeneous brittle materials, *International Journal for Numerical and Analytical Methods in Engineering*, *90(8)*, 1053–1072.

Hantschel, T., and I. K. Armin (2009), *Fundamentals of Basin and Petroleum System Modeling*, Springer.

Hild, F. (2001), *Probabilistic approach to fracture: the Weibull model*, In Handbook of materials behavior models.

Kim, J., H. Tchelepi, and R. Juanes (2010), Stability accuracy and efficiency of sequential methods for coupled flow and geomechanics, in *SPE Reservoir simulation symposium. The Woodlands, Texas*.

Longuemare, P., M. Mainguy, P. Lemonnier, A. Onaisi, C. Gerard, and N. Koutsabeloulis (2002), Geomechanics in reservoir simulation: Overview of coupling methods and field case study, *Oil & Gas Science and Technology - Rev. IFP*, *57*, 471–483.

Luo, X., and G. Vasseur (2002), Natural hydraulic cracking: Numerical model and sensitivity study, *Earth and Planetary Science Letters*, *201*, 431–446.

Lynton, S., K. L. Milliken, and F. M. Earle (1987), Diagenetic evolution of cenozoid sandstones gulf of mexico sedimentary basin, *Sedimentary geology*, *50*, 195–225.

Miall, A. (2000), *Principles of Sedimentary Basin Analysis*, Springer.

Mourgues, R., J. Gressier, L. Bodet, D. Bureau, and A. Gay (2011), Basin scale versus localized pore pressure/stress coupling -implications for trap integrity evaluation, *Marine and Petroleum Geology*, *28*, 1111–1121.

Neuzil, C. (2003), Hydromechanical coupling in geologic process, *Hydrogeology Journal*, *11*, 41–83.

Pouya, A. (2012), Three-dimensional flow in fractured porous media: A potential solution based on singular integral equations, *Advances in Water Ressources*, *35*, 30–40.

Pouya, A. (2015), A finite element method for modeling coupled flow and deformation in porous fractured media, *International Journal for Numerical and Analytical Methods in Geomechanic*, *39*, 1836–1852.

Pouya, A., and Y. Bemani (2015), A damage-plasticity model for cohesive fractures, *International Journal for Rock Mechanics & Minning Sciences*, *73*, 194–202.

Pouya, A., and S. Ghabezloo (2010), Flow around a crack in a porous matrix and related problems, *Transport in Porous Media*, *84*, 511–532.

Renshaw, C., and C. Harvey (1994), Propagation velocity of a natural hydraulic in a poroelastic medium, *Journal of Geophysical Research*, *99, No B11*, 21,667–21,677.

Roberts, S., and J. Num (1995), Episodic fluid expulsion from geopressured sediments, *Marine and Petroleum Geology*, *12*, 195–204.

Rozhko, A. (2016), Two-phase fluid -flow in a dilatant crack-line pathway, *Journal of Petroleum Science & Engineering*, *146*, 1158–1172.

Rozhko, A., Y. Podladchikov, and F. Renard (2007), Failure patterns caused by localized rise in pore-fluid overpressure and effective strength of rocks, *Geophysical Research Letters*, *34*, L22,304.

Rutqvist, J., and O. Stephansson (2003), The role of hydromechanical coupling in fracatured rock engineering, *Hydrogeology Journal*, *11*, 7–40.

Schneider, F., M. Bouteca, and J. Sarda (1999), Hydraulic fracturing at sedimentary basin scale, *Oil & Gas Science and Technology*, *54, No 6*, 797–806.

Secor, D. (1965), Role of fluid pressure in jointing, *American Journal of Science*, *263*, 633–646.

Secor, D. (1969), Mechanisms of natural extension fracturing at depth in the earth's crust, *Geological Survey of Canada Paper*, *68-52*, 3–48.

Sibson, R. (2003), Brittle failure controls on maximul sustainable overpressure in different tectonic regimes., *AAPG Bulletin*, *87 (6)*, 901–908.

Terzaghi, K. (1936), The shearing resistance of saturated soils, *In: Proceedings of the first international conference on Soil Mechanics and Foundation Engineering*, pp. 85–94.

Touloukian, Y. S., W. R. Judd, and R. F. Roy (1989), *Physical properties of rocks and minerals*, Hemisphere, Bristol.

Turcotte, D. L., and M. Glasscoe (2004), A damage model for the continuum rheology of the upper continental crust, *Tectonophysics*, *383*, 71–80.

Twenhofen, W. (1950), *Principles of sedimentation*, Mc Graw-Hill Book company.

Weibull, W. (1939), *A statistical theory of the strength of materials*, Royal Swedish Institute for Engineering Research.